energies

MDPI

Article

Enhanced Bio-Oil Yield from Thermal Decomposition of Peanut Shells Using Termite Hill as the Catalyst

Jan Nisar [1,*], Ali Ahmad [1], Ghulam Ali [1], Nafees Ur Rehman [1], Afzal Shah [2,*] and Iltaf Shah [3,*]

[1] National Centre of Excellence in Physical Chemistry, University of Peshawar, Peshawar 25120, Pakistan; aliahmaddawar485@gmail.com (A.A.); ghulamali@uop.edu.pk (G.A.); nafeesrehman141@gmail.com (N.U.R.)
[2] Department of Chemistry, Quaid-i-Azam University, Islamabad 45320, Pakistan
[3] Department of Chemistry, College of Science, United Arab Emirates University, Al-Ain P.O. Box 15551, United Arab Emirates
* Correspondence: pashkalawati@gmail.com (J.N.); afzalshah@qau.edu.pk or afzals_qau@yahoo.com (A.S.); altafshah@uaeu.ac.ae (I.S.)

Abstract: This study focused on the thermal degradation of peanut shells in the presence and absence of a termite hill as the catalyst. EDX, XRF, SEM, SAA and XRD were employed for the characterization of the termite hill. The bio-oil obtained from peanut shell pyrolysis was analyzed by GC-MS. To ascertain the kinetic parameters of the reaction, thermogravimetric analysis of peanut shells was carried out with and without a termite hill at heating rates of 3, 12, 20 and 30 °C·min^{-1}. TG/DTG of peanut shells revealed four steps of weight loss from 30 to 800 °C. The weight loss was attributed to the evaporation of water and degradation of hemicellulose, cellulose and lignin. The Kissinger method was applied for the evaluation of kinetic parameters. The activation energy (E) for the non-catalyzed degradation reactions of hemicellulose, cellulose and lignin was evaluated as 108.082, 116.396 and 182.908 kJ/mol, with a pre-exponential factor (A) of 1.9×10^8, 2.42×10^9 and 2.98×10^{11} min^{-1}, respectively. Similarly, for the catalyzed reaction, the values of E and A were calculated as 66.512, 74.826 and 133.024 kJ/mol and 5.83×10^6, 2.859×10^7 and 1.46×10^9 min^{-1}, respectively. The termite hill not only reduced the degradation temperature and activation energy but also modified the composition of the bio-oil. In the case of the non-catalyzed reaction, the bio-oil was found to consist of C_5-C_{24}, while catalytic pyrolysis produced more components ranging from C_4 to C_{31} hydrocarbons.

Keywords: biomass; waste management; pyrolysis; biofuel; kinetics; activation energy

Citation: Nisar, J.; Ahmad, A.; Ali, G.; Rehman, N.U.; Shah, A.; Shah, I. Enhanced Bio-Oil Yield from Thermal Decomposition of Peanut Shells Using Termite Hill as the Catalyst. *Energies* **2022**, *15*, 1891. https://doi.org/10.3390/en15051891

Academic Editor: Attilio Converti

Received: 19 January 2022
Accepted: 27 February 2022
Published: 4 March 2022

1. Introduction

Energy resources fall into three classes, i.e., fossil fuels, nuclear and renewable resources [1]. The world's major energy resource is fossil fuels; however, these are rapidly exhausting owing to booming industrialization and technological advancement [2]. Almost every country in the world is facing an energy crisis, and in order to fill the gap between supply and demand, researchers are searching for renewable, sustainable and energy-efficient sources [3]. The increase in emission of toxic gases from fossil fuel combustion is an issue of grave concern in the context of climate change [4]. Consequently, economic and environmental dilemmas have been created due to the over-consumption of non-renewable fossil fuels. To beat this challenge, a plethora of research groups worldwide are looking for alternative energy resources that could be renewable, cost-affordable and environmentally friendly resources [5]. Nuclear power contributes about 13% of electrical energy to the worldwide demand. As a result of the Chernobyl nuclear power plant incident in 1986, nuclear power plants are not considered suitable for energy generation [6]. Various challenges need to be effectively settled for this source of energy to make further advancements in safety, reliability, vulnerability and economic feasibility [7].

Renewable sources, i.e., solar energy, wind energy, biomass energy and geothermal energy, can provide energy contributions with zero or nearly zero outflows of both air contaminants and ozone-harming substances [8]. Thus, the utilization of environmentally friendly renewable sources can fill the gap between supply and demand. Currently, biomass conversion to energy has caught the attention of researchers, as biomass waste is cheap and easily available. Therefore, many research groups are engaged worldwide in finding a suitable method for biomass conversion into useful energy with low contamination risks.

Peanut (botanical name "*ArachisHypogaea* L.") is the world's third most significant source of vegetable protein feed, and the fourth most crucial source of palatable vegetable oil [9]. In 2019, global production of peanuts reached 45.06 million tons/year. Asia produced 60.6% in that period, followed by Africa with 29.2%, America with 10.1% and Oceania with 0.1% [10]. In the US, about 70% of the crop is eaten locally or exported as peanut butter, peanut kernels and confections, while in some countries of the world, such as Brazil, Senegal, Argentina and India, more than 75% of the peanut crop is crushed or exported for utilization as oil and animal feed [9].

A tremendous amount of waste is produced worldwide every day due to the consumption of the edible part of the peanut and the discarding of the shell. This has attracted the attention of various researchers who are focusing on ways to convert shells into valuable components. Zhang et al. [11] investigated the degradation of peanut shells in a fluidized bed via fast pyrolysis, and the oil collected was examined by gas chromatography mass spectrometry (GC-MS). The characteristics of the bio-oil and the distribution of products were correlated with the carrier gas flow rate and reaction temperature. They classified the main bio-oil components into six categories: ketones, esters, aldehydes, phenols, acids and alcohols. The authors stated that at the 3.2 Nm^3h^{-1} flow rate of N_2 gas at 500 °C, the oil yield reached a maximum, i.e., around 60% by weight.

Messina et al. [12] examined the decomposition of peanut shells that were pretreated with acid to improve bio-oil yield. For comparison, pristine shell pyrolysis was also studied. The maximum oil yield was obtained for both samples at 500 °C; however, pretreated acid shells gave more bio-oil than pristine shells. Mamaeva et al. [13] investigated the degradation of peanut shells using NaOH, Fe_3O_4, KOH and Na_2CO_3 as catalysts. They examined the impacts of catalyst type, biomass/catalyst ratio and temperature on the bio-oil composition. Using Na_2CO_3 as a catalyst remarkably increased the phenols in the bio-oil. NaOH and KOH resulted in elevated heating values while lowering the oxygen content. Torres-García et al. [10] conducted a thermo-kinetic analysis of peanut shells. Three models were applied to the thermogravimetric data, namely, Friedman (Fr), Kissinger (K) and Kissinger–Akahira–Sunnose (KAS), to find an effective activation energy amid the pyrolysis process. The results obtained from the pyrolytic breakdown of peanut shells applying the Kissinger model revealed the non-dependence of the pyrolysis reaction on the heating rate, and simple first-order kinetics was proposed for the degradation reaction.

Peanuts are abundantly grown in Pakistan and eaten extensively throughout the country by all and sundry due to their low price compared to other dry fruits. The peanut crop is mainly grown in rain-fed areas of Punjab, Khyber Pakhtunkhwa and Sind. According to a recent survey, peanut is a priority food in Pakistan, due to its high nutritional value, low price and easy availability. After eating the edible parts, the shells, which are vital lignocellulosic material, are thrown away as waste. Substantial research has been carried out on the conversion of various biomasses to bio-oil; however, studies on the kinetics and pyrolysis of peanut shells are very scant [10,13]. Therefore, the aim of this research work was to convert peanut shell waste into valuable products using a pyrolysis technique, and to study the kinetics of both catalytic and non-catalytic pyrolysis reactions of peanut shell waste.

2. Material and Methods

2.1. Materials

Peanuts were purchased from a dry fruit market at Ashraf Road Peshawar, Khyber Pakhtunkhwa, Pakistan. After the utilization of the eatable portion, the waste shells were

collected and dried in sunlight for two weeks. The peanut shells were then ground well in a grinder and sieved to a mesh size of 35.

Keeping in view the anticipated properties of the catalyst, among various natural wastes, a termite hill was selected. The termite hill was ground in a pestle and mortar and converted into powder form. The powder form catalyst was stored in a capped bottle for further study. The condenser, Pyrex glass reaction vessel and connecting pipe were washed frequently in acetone after pyrolysis experiments.

2.2. Characterization of Catalyst

The morphology of the sample was analyzed using a scanning electron microscope (SEM)(JSM-IT-100, JEOL, Akishima, Tokyo, Japan), and the elemental composition was analyzed with a backscattered EDS (energy-dispersive spectroscopy) detector integrated into the SEM. An X-ray fluorescence spectrometer (XRF) (EDX 7000 Shimadzu, Nakagyo-Ku, Kyoto, Japan) was used to find the compound composition of the sample. An X-ray diffractometer (XRD) (JDX-3532 JEOL, Akishima, Tokyo, Japan) with Cu Kα radiation was used to ascertain its crystalline phase using X'pert High Score software. Intensities vs. 2θ were plotted, where Scherrer's equation was used for the crystal size calculation. A surface area and pore size analyzer (NOVA2200e Quantachrome, Boynton Beach, FL, USA) was utilized for the calculation of the surface area, pore volume and pore radius of the catalyst.

2.3. Pyrolysis-GC/MS

Pyrolysis of peanut shells without a termite hill and with a termite hill in the ratio of 95:5 was performed in a salt bath which was heated by a coil heater inside the bath. A sketch of the pyrolysis setup has already been presented in our previous communication [14]. The temperature was monitored by a controller with a thermocouple. All the pyrolysis experiments were performed in a Pyrex vessel in the absence of oxygen and in an inert atmosphere of nitrogen. After the completion of the reaction, the bio-oil was collected and weighed. The weight of biochar was determined from the weight difference between the reaction vessel with biochar and the empty vessel. The percentage of gases produced was measured by 100 − (%bio-oil + %biochar). The oil obtained was analyzed using GC-MS (QP2010 Ultra, Shimadzu, Nakagyo Ward, Kyoto, Japan).

2.4. Kinetic Study

Thermogravimetric analysis was performed for peanut shell powder with/without a catalyst at heating rates of 3, 12, 20 and 30 °C·min^{-1} from 30 to 800 °C, using a thermogravimetric analyzer (TGA Q 500 TA, New Castle, DE, USA) in nitrogen gas with a flow rate of 20 mL/min. The obtained data were used for measuring the kinetic parameters using the following Kissinger equation:

$$\ln\left[\frac{\beta}{T_m^2}\right] = \ln\left(\frac{A.R}{E}\right) - \frac{E}{RT_m} \quad (1)$$

where T_m represents the maximum decomposition temperature. By plotting $\ln\left(\frac{\beta}{T_m^2}\right)$ on the *y*-axis vs. $\frac{1000}{T_m}$ on the *x*-axis, the E and A values were calculated from the slope and intercept of the plots [15].

3. Results and Discussion

3.1. Catalyst Characterization

Figure 1 exhibits an SEM image, which was carried out for the determination of the surface texture of the termite hill catalyst. The figure demonstrates irregularly distributed minerals present in the termite hill, with granular as well as homogenous structures; some of them are rod-shaped, and in some places, they are in the form of an agglomerated mass. These particles also vary in size. Some are very small, while others are bigger in size. These structures were micro-sized, with a mean area of 0.506 μm^2 and a mean length of

13.536 µm, which was determined via ImageJ software. Moreover, the SEM image reflects the porous surface of the catalyst. The outcomes are in line with previous revelations. Millogo et al. [16] carried out SEM of a termite hill and noted that the surface of the sample had a homogenous microstructure composed of large quartz grains linked by irregular kaolinite particles. Ayanda et al. [17] showed that the termite hill consisted of crystalline, rod-like particles of α-quartz silica with various shapes.

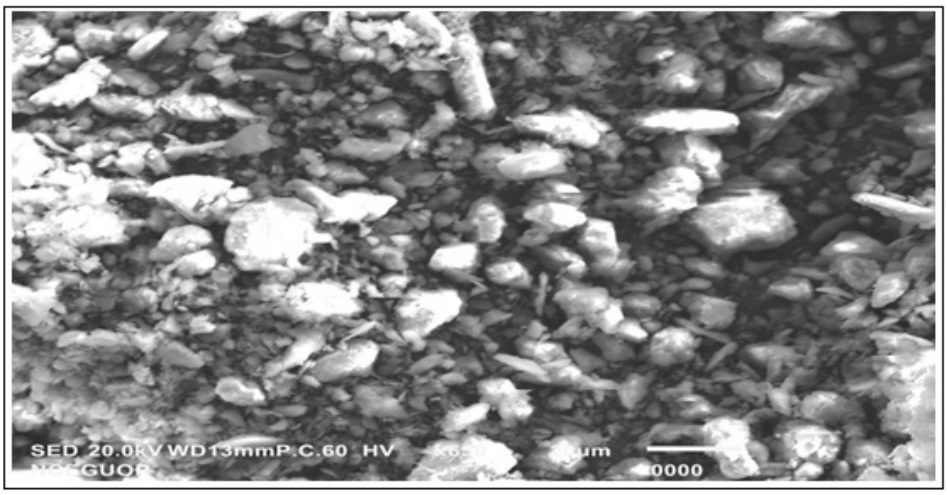

Figure 1. SEM image of the termite hill.

Figure 2 presents the chemical composition of the termite hill with the atom% of oxygen (55.71%), carbon (28.81%), silicon (9.8%), aluminum (3.77%), iron (1.15%), magnesium (0.73%) and potassium (0.65%). The data obtained are somewhat in agreement with reported studies. Ayanda et al. [17] performed EDX analysis of a termite hill and found that the sample was rich in oxygen (59.9%), followed by carbon (20.4%), silicon (11.66%), aluminum (7.92%) and other elements in trace amounts. Mahamat and Azeko [18] performed EDX analysis of the different compositions of termite soil and observed the existence of calcium, silicon, iron and aluminum in different quantities. These analyses indicate that termite hills' composition depends on the soil location.

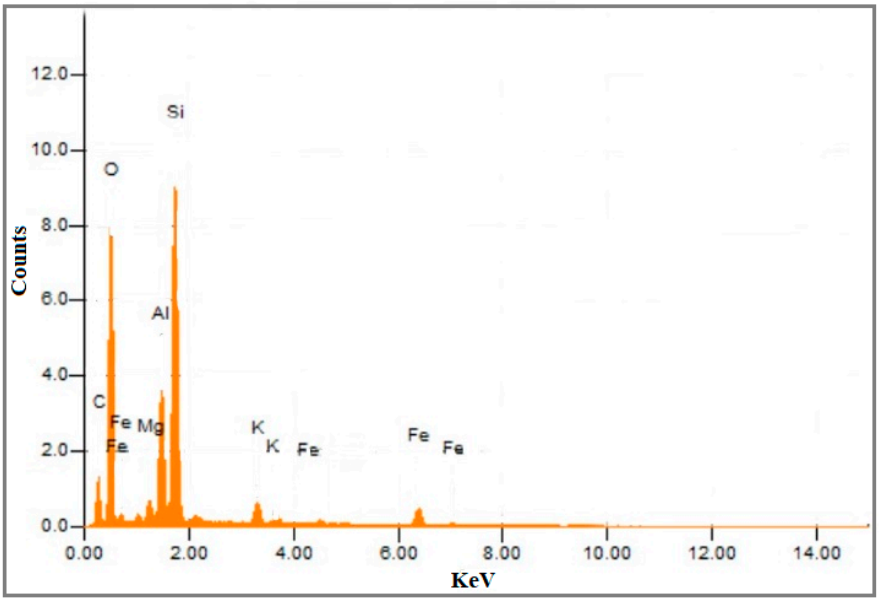

Figure 2. EDX analysis of the termite hill.

The termite hill was also analyzed using XRF. It was found to be rich in silica, alumina, potassium oxide, calcium oxide, titanium oxide, sulfur oxide, vanadium oxide and chromium oxide, with percentages of 69.030, 21.990, 4.154, 3.342, 1.273, 0.120, 0.053 and 0.037%, respectively, as shown in Table 1. The data obtained from XRF analysis are in consonance with the results obtained from EDS. Some of the abandoned naturally occurring materials have the potential to catalyze a reaction. To explore the catalytic potential of such materials, Yusuff et al. [19] revealed that a titania-termite hill composite is a good catalyst for transesterification of spilth cooking oil. The authors studied the XRF of a termite hill and found SiO_2, Al_2O_3, CaO, MgO, TiO_2, K_2O, Na_2O and Fe_2O_3, with percentages of 51.92, 21.62, 11.43, 1.32, 2.16, 1.31, 0.63 and 8.55%, respectively.

Table 1. XRF analysis showing %age of different compounds in a termite hill.

S.No	Compound	%Age
01	SiO_2	69.030
02	Al_2O_3	21.990
03	K_2O	4.154
04	CaO	3.342
05	TiO	1.273
06	SO_3	0.120
07	V_2O_5	0.053
08	Cr_2O_3	0.037

In another study, Yusuff [20] investigated whether TiO_2/termite hill can be used as a photocatalyst for the degradation of methylene blue dye, which is a waste effluent of the textile industries. Ayanda et al. [17] analyzed the XRF of a termite hill and found iron oxide in abundance (23.8%), followed by silica oxide (20.6%) and alumina (14.4%), while Ti, V, Mn, Co, Fe, etc., were observed in lesser amounts.Folorunso et al. [21] performed XRF of a termite hill and found SiO_2 (65.18%), Al_2O_3 (24.56%), CaO (6.27%), Fe_2O_3 (1.28%), MgO (0.7%), K_2O (0.09%), Na_2O (0.84%), TiO_2 (0.68%), Cr_2O_3 (0.03%), P_2O_5 (0.02%) and ZrO_2 (0.1%).

In order to ascertain the surface characteristics, surface area analysis of the termite hill was carried out usinga surface area and pore size analyzer. Applying the Barrett–Joyner–Halenda (BJH) adsorption method, the pore volume, pore radius and surface area of the termite hill were calculated to be 0.004 cm^3/g, 17.015 Å and 5.065 m^2/g, respectively, while the specific surface area of the termite hill was determined to be 34.637 m^2/g using the BET surface area analysis method. The results agree well with previous investigations. Yusuff et al. [22] studied the textural properties of a termite hill and calculated the BET surface area as 13.24 m^2/g, pore volume as 0.053 cm^3/g and pore diameter as 15.79 Å.

Various basic components were identified with different crystalline phases in XRD analysis of the termite hill, as shown in Figure 3. XRD data were inserted in X'pert High Score software, and crystalline phases of the oxides of different metals of the sample were found from XRD analysis. It was found that oxides of silicon and aluminum are Boggsite with the orthorhombic crystal system [23], Chabazite-Ca with the hexagonal crystal system [24] and Sillimanite with the orthorhombic crystal system [25]. Similarly, oxides of titanium and iron identified from the XRD measurements have different phases: $Ti_{168}O_{456}$ has a cubic structure [26], Titanium(III) oxide has a hexagonal structure [27], Baddeleyite has a monoclinic structure [28], Fe_3O_4 has an orthorhombic structure and Maghemite has a cubic structure [29]. Scherrer's formula given in Equation (2) was used for the measurement of the mean crystallite size, and the average crystallite size was observed to be 21.75 nm, which agrees well with reported studies. Yusuff [20] doped titania on a termite hill and measured the crystallite size as 17.10 nm. In another study, Yussuf et al. [22] measured the crystallite size of a ZnO-doped termite hill as 27.6 nm.

$$Dp = \frac{k\lambda}{\beta \cos \theta} \quad (2)$$

where Dp is the mean crystallite size, λ represents the X-ray wavelength, β is line broadening in radians/full width half maximum (FWHM), θ is the Bragg angle and k is a constant having a value equal to 0.94 [30]. The data obtained are in line with earlier studies. Millogo et al. [31] studied termite hill mineralogy and microstructure, and from XRD analysis, the authors found microcline ($KAlSi_3O_8$), quartz (SiO_2) and K-feldspar ($KAlSi_3O_8$–$NaAlSi_3O_8$–$CaAl_2Si_2O_8$) as the main constituents. Mujinya et al. [32] examined a termite hill's composition and properties, and the XRD data revealed that the termite hill contained goethite (Iron (III) oxide) with an orthorhombic crystal structure, hematite (Fe_2O_3) and quartz (SiO_2). These supporting contents confirm that our XRD analysis is in conformity with the reported research approach, and the small differences might be due to the sampling location and the software used in the XRD data interpretation.

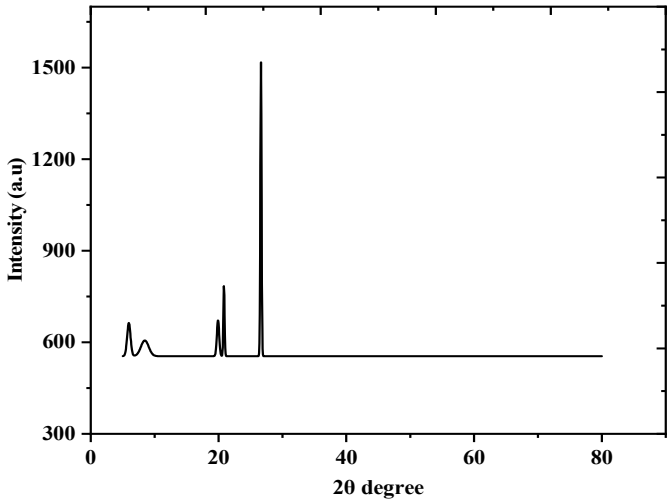

Figure 3. XRD of the termite hill.

3.2. Pyrolysis of Peanut Shells and Bio-Oil Characterization

Temperature plays a very eminent role in converting biomass into valuable products. Amid pyrolysis, varying amounts of products are produced, and their distribution is affected by the reaction temperature. Figure 4a reflects the non-catalytic pyrolysis of peanut shells, with the oil content gradually increasing and reaching a peak at 350 °C. In addition, the amount of oil decreases with increasing temperature beyond 350 °C. Hence, the optimal temperature at which the maximum recovery was obtained is 350 °C. It was noted that the gaseous fraction improved with elevated temperature, which can be ascribed to the secondary decomposition of the condensable components formed [33]. Figure 4b shows the catalytic degradation of peanut shells at different temperatures. It can be observed from the graph that when the temperature reaches 330 °C, the maximum liquid product is obtained and then decreases. Hence, the optimum temperature is 330 °C for liquid formation. This reveals that the termite hill catalyst maximized oil production and lowered the optimal temperature to 330 °C as well. These observations are in consonance with the findings of Aho et al. [34]. The authors investigated the thermal degradation of biomass over a zeolite and observed a higher yield of pyrolysis oil. Figure 4c shows the effect of different ratios of catalyst to biomass on pyrolysis products. As can be observed from the figure, with an increase in catalyst loading from 1 to 5%, the bio-oil yield is enhanced and then decreases. This indicates that an increase in catalyst loading favors liquefaction; however, it has a negative effect beyond an optimum level of 5%. This is due to the fact that, with an increase in catalyst loading, the bio-oil molecules are easily adsorbed on the high specific surface area of the catalyst, leading to catalyst poisoning.

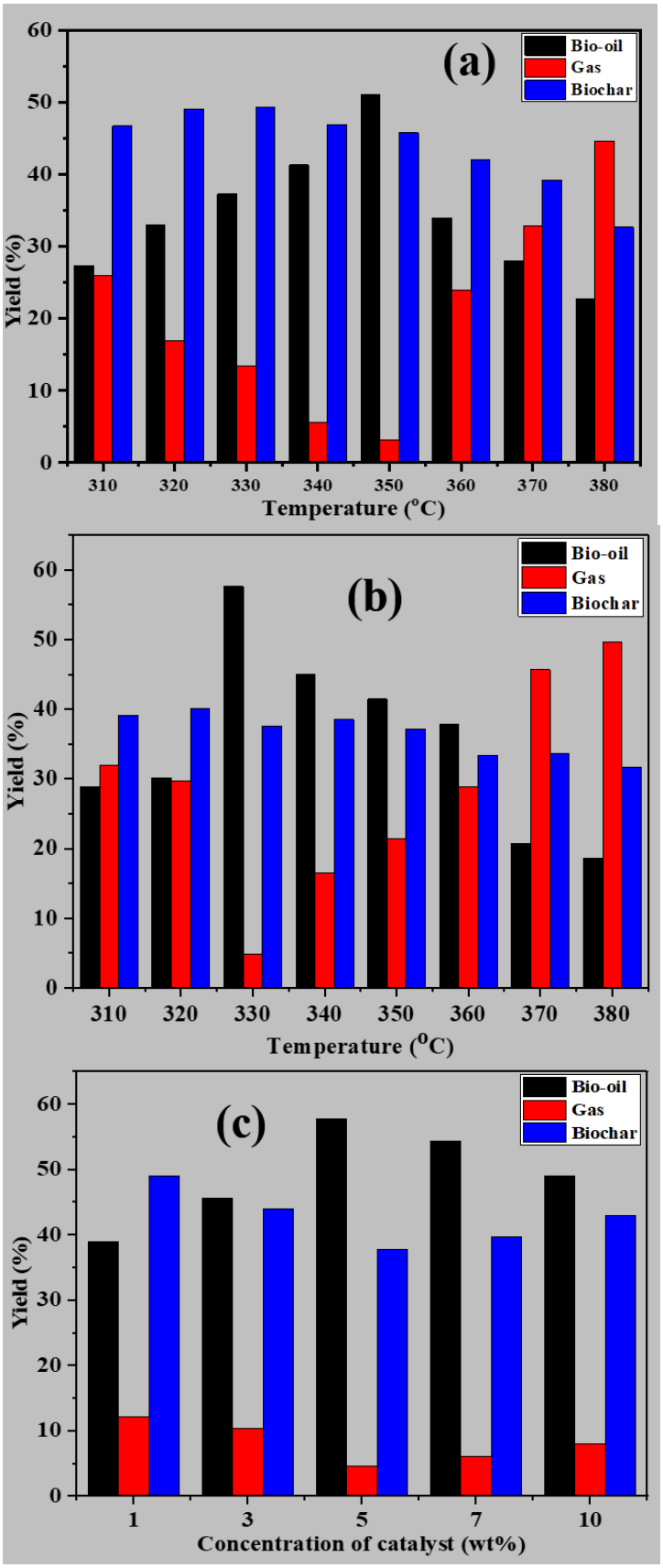

Figure 4. Influence of temperature and catalyst on pyrolysis products: (**a**) without a catalyst; (**b**) with a catalyst; (**c**) catalyst concentration.

In order to examine the composition of the pyrolysis oil, GC-MS of the oil obtained from non-catalyzed and catalyzed reactions was performed. The obtained chromatograms are depicted in Figure 5a,b, and all the compounds, with their names, retention times, chemical formula, percent area and molecular weights, detected in the oil are shown in Table 2. The bio-oil recovered from the non-catalyzed degradation of peanut shells contains hydrocarbons in the range of C_3–C_{24}. The main components identified in the pyrolysis oil were 2-methoxy-phenol, 2-furanmethanol, 2-methoxy-4-phenol, furfural, 2-methoxy-4-vinylphenol, 4-ethyl-2-methoxy-phenol and lactose. In the presence of the termite hill catalyst, the pyrolysis of peanut shells produced a change in the nature and chemical composition of the bio-oil, when compared with the bio-oil obtained from the pyrolysis of solitary peanut shells, i.e., C_4–C_{31} hydrocarbons were detected for catalytic pyrolysis. The major hydrocarbons detected include 1-(4-hydroxy-3-methoxyphenyl)-propanone, tetrahydro [2,2′]bifuranyl-5-one, 1,2-benzenediol, cyclopropyl carbinol and 1-(4-hydroxy-3-methoxyphenyl)-ethanone. Hence, it was revealed that the termite hill played an effective role as a catalyst for improving the quality of the oil. These findings are in agreement with reported investigations.

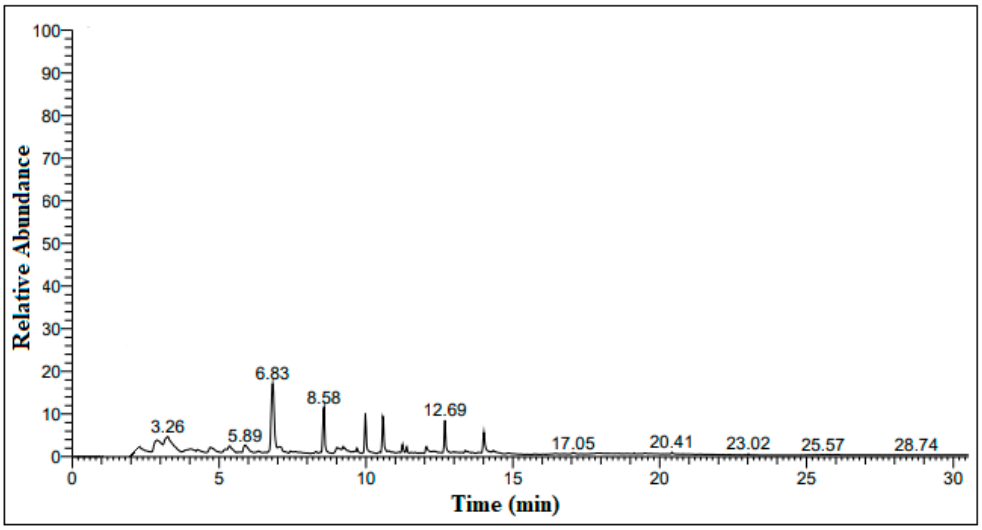

(**a**)

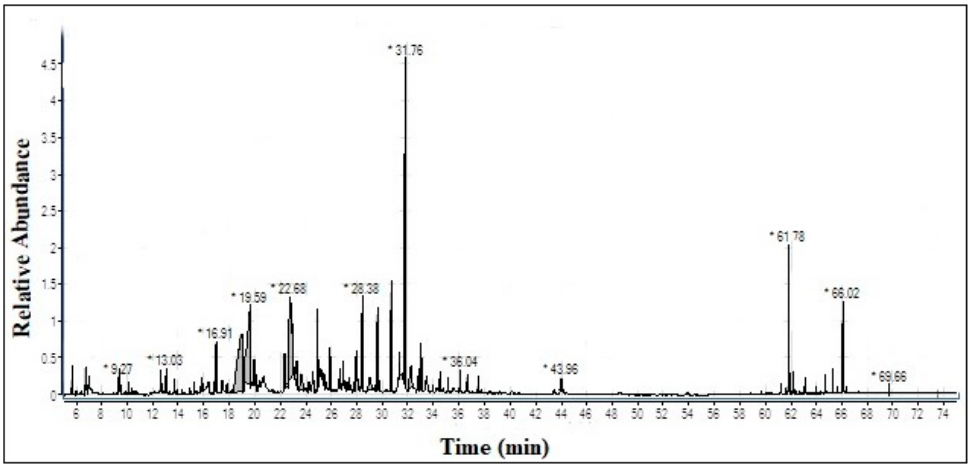

(**b**)

Figure 5. (**a**) GC/MS of bio-oil obtained from peanut shell pyrolysis without a catalyst. (**b**) GC/MS of bio-oil obtained from peanut shell pyrolysis with a catalyst.

Table 2. (**a**) Components detected in oil obtained from the non-catalyzed reaction of peanut shells. (**b**) Components detected in oil obtained from the catalyzed reaction of peanut shells.

S.No	R/Time	Component	Chem. Formula	M.wt.	%Area
		(**a**)			
1	2.26	Pentanoic acid, 4-methyl-	$C_6H_{12}O_2$	116	2.081833
2	2.89	Furfural	$C_5H_4O_2$	96	8.101473
3	3.26	2-Furanmethanol	$C_5H_6O_2$	98	12.11129
4	4.05	Cyclohexanol, 2,4-dimethyl-	$C_8H_{16}O$	128	2.864157
5	4.71	2-Furancarboxaldehyde, 5-methyl-	$C_6H_6O_2$	110	2.536825
6	5.36	1-Hydroxy-2-pentanone	$C_5H_{10}O_2$	102	3.436989
7	5.89	1,2-Cyclopentanedione, 3-methyl-	$C_6H_8O_2$	112	3.191489
8	6.34	1,2-Butanediol, 1-phenyl-	$C_{10}H_{14}O_2$	166	1.163666
9	6.83	Phenol, 2-methoxy-	$C_7H_8O_2$	124	24.05892
10	7.44	Undecanoic acid, hydroxy-, lactone	$C_{11}H_{20}O_2$	184	1.572831
11	8.58	Phenol, 2-methoxy-4-methyl-	$C_8H_{10}O_2$	138	9.001637
12	9.23	Lactose	$C_{12}H_{22}O_{11}$	342	5.237316
13	9.98	Phenol, 4-ethyl-2-methoxy-	$C_9H_{12}O_2$	152	6.382979
14	10.57	2-Methoxy-4-vinylphenol	$C_9H_{10}O_2$	150	6.95581
15	11.25	Phenol, 2-methoxy-6-(2-propenyl)-	$C_{10}H_{12}O_2$	164	1.14566
16	12.06	Phenol, 2-methoxy-5-(1-propenyl)-	$C_{10}H_{12}O_2$	164	2.209493
17	12.69	Phenol, 2-methoxy-4-(1-propenyl)-	$C_{10}H_{12}O_2$	164	4.746318
18	13.38	Ethanone, 1-(4-hydroxy-3-methoxyphenyl)-	$C_9H_{10}O_3$	166	0.490998
19	14.34	3-Lauramidobenzoic acid	$C_{19}H_{29}NO_3$	319	0.736498
20	17.05	Tertubryn	$C_{10}H_{19}N_5S$	241	0.163666
21	20.41	10-Octadecenoic acid, methyl ester	$C_{19}H_{36}O_2$	296	0.163666
22	23.02	1,2-Benzenedicarboxylic acid, diisooctyl ester	$C_{24}H_{38}O_4$	390	0.081833
		(**b**)			
1	5.6	p-Dioxane-2,3-diol	$C_4H_8O_4$	120	0.57
2	9.27	Ethane, 1,2-bis[(4-amino-3-furazanyl)oxy]-	$C_6H_8N_6O_4$	228	0.37
3	12.57	Cyclopentanone	C_5H_8O	84	0.56
4	13.03	1,2-Cyclopentanedione	$C_5H_6O_2$	98	0.6
5	13.65	2,5-Furandione, 3-methyl-	$C_5H_4O_3$	112	0.31
6	15.82	Pyridine, 3-methoxy-	C_6H_7NO	109	0.26
7	16.91	1,2-Cyclopentanedione, 3-methyl-	$C_6H_8O_2$	112	2.53
8	18.84	Tetrahydro[2,2′]bifuranyl-5-one	$C_8H_{12}O_3$	156	13.22
9	19.59	Cyclopropyl carbinol	C_4H_8O	72	11.36
10	19.9	Maltol	$C_6H_6O_3$	126	0.75
11	22.27	Phenol, 2-methoxy-4-methyl-	$C_8H_{10}O_2$	138	0.74
12	22.68	1,2-Benzenediol	$C_6H_6O_2$	110	12.72
13	23.21	1,4:3,6-Dianhydro-α-d-glucopyranose	$C_6H_8O_4$	144	1.25
14	23.58	Furancarboxaldehyde, 5-(hydroxymethyl)-	$C_6H_6O_3$	126	1.62
15	24.84	Phenol, 4-ethyl-2-methoxy-	$C_9H_{12}O_2$	152	2
16	25.86	2-Methoxy-4-vinylphenol	$C_9H_{10}O_2$	150	1
17	26.62	2(3H)-Furanone, 5-heptyldihydro-	$C_{11}H_{20}O_2$	184	0.72
18	26.86	2,4-Dimethoxyphenol	$C_8H_{10}O_3$	154	1.01
19	27.3	Benzenemethanol, α-ethyl-4-methoxy-	$C_{10}H_{14}O_2$	166	0.22
20	27.89	4-Ethylcatechol	$C_8H_{10}O_2$	138	1.13
21	28.38	Benzaldehyde, 3-hydroxy-4-methoxy-	$C_8H_8O_3$	152	3.79
22	28.95	d-Mannose	$C_6H_{12}O_6$	180	1.74
23	29.54	Phenol, 2-methoxy-4-(1-propenyl)-, (Z)-	$C_{10}H_{12}O_2$	164	2.22
24	29.64	Ascaridole epoxide	$C_{10}H_{16}O_3$	184	0.33
25	30.63	Ethanone, 1-(4-hydroxy-3-methoxyphenyl)-	$C_9H_{10}O_3$	166	4.65
26	31.26	Benzoic acid, 4-hydroxy-3-methoxy-, methyl ester	$C_9H_{10}O_4$	182	0.5
27	31.76	Propanone, 1-(4-hydroxy-3-methoxyphenyl)-	$C_{10}H_{12}O_3$	180	16.87
28	32.19	Guanosine	$C_{10}H_{13}N_5O_5$	283	2.42
29	32.74	9-Ethoxy-10-oxatricyclo[7.2.1.0(1,6)]dodecan-11-one	$C_{13}H_{20}O_3$	224	0.32
30	32.92	1,2-Dimethoxy-4-n-propylbenzene	$C_{11}H_{16}O_2$	180	1.1
31	33.02	3-Benzofuranmethanol, 2,3-dihydro-2-(4-hydroxy-3-methoxyphenyl)-5-(3-hydroxy-1-propenyl)-7-methoxy-	$C_{20}H_{22}O_6$	358	0.74
32	34.46	Phenylacetylformic acid, 4-hydroxy-3-methoxy-	$C_{10}H_{10}O_5$	210	0.73
33	35.1	Benzenesulfonamide, 2-nitro-N-[2-(4-pyridinyl)ethyl]-	$C_{13}H_{13}N_3O_4S$	307	0.27
34	36.04	4-Hydroxy-2-methoxycinnamaldehyde	$C_{10}H_{10}O_3$	178	0.65
35	36.59	1,2-Cycloheptanedione, 3,3,7,7-tetramethyl-, dihydrazone	$C_{11}H_{22}N_4$	210	0.55
36	37.44	5,10-Diethoxy-2,3,7,8-tetrahydro-1H,6H-dipyrrolo[1,2-a;1′,2′-d]pyrazine	$C_{14}H_{22}N_2O_2$	250	0.54
37	43.96	Tetradecanoic acid, 3,3a,4,6a,7,8,9,10,10a,10b-decahydro-3a,10a-dihydroxy-5-(hydroxymethyl)-2,10-dimethyl-3-oxobenz[e]azulen-8-yl ester, [3aR-(3aα,6aα,8α,10β,10aβ,10bβ)]-	$C_{31}H_{50}O_6$	518	0.95

Table 2. *Cont.*

S.No	R/Time	Component	Chem. Formula	M.wt.	%Area
38	61.18	Ethyl homovanillate	$C_{11}H_{14}O_4$	210	0.25
39	61.78	Hydroxy-4-(1-methoxycyclopropyl)-3,3,5,8,10,10-hexamethyltricyclo[6.2.2.0(2,7)]dodeca-5,11-dien-9-one	$C_{22}H_{32}O_3$	344	4.17
40	62.11	Phenol, 2,2′-methylenebis[6-(1,1-dimethylethyl)-4-methyl-	$C_{23}H_{32}O_2$	340	0.48
41	63.1	6,7-Epoxypregn-4-ene-9,11,18-triol-3,20-dione, 11,18-diacetate	$C_{25}H_{32}O_8$	460	0.46
42	64.64	6,7-Epoxypregn-4-ene-9,11,18-triol-3,20-dione, 11,18-diacetate	$C_{25}H_{32}O_8$	460	0.37
43	65.21	10,11-Dihydro-10-hydroxy-2,3-dimethoxydibenz(b,f)oxepin	$C_{16}H_{16}O_4$	272	0.51
44	66.02	1,2-Benzenedicarboxylic acid, diisooctyl ester	$C_{24}H_{38}O_4$	390	2.14

Zhang et al. [11] reported aldehydes, ketones, alcohols, esters and acids as major compounds in oil collected from pyrolysis of peanut shells. The authors listed 1-hydroxy-2-pentanone, phenol, 2-cyclopenten-1-one, 4-ethyl-2-methoxy, 2-hydroxy-3-methyl, etc., as major compounds. Messina et al. [35] studied the pyrolysis of peanut shells over a modified natural zeolite. They found 2-methoxy-4-methylphenol, 2-methoxy-4-propylphenol, 2-methoxyphenol and 5-hydroxymethylfurfural as the main constituents.

3.3. Kinetic Study

Peanut shells were pyrolyzed with and without a termite hill at heating rates of 3, 12, 20 and 30 °C·min^{-1}, and the kinetic parameters were measured using the Kissinger method. Kinetic parameters for hemicellulose, cellulose and lignin degradation were calculated from the plot depicted in Figure 6a,b, and these are listed in Table 3. The observations agree well with earlier studies. Lopez-Velazquez et al. [36] carried out pyrolysis of lignocellulosic biomass. They noted three actual degradation steps, i.e., degradation of hemicellulose, cellulose and lignin. Yang et al. [37] performed decomposition of biomass and assigned the three degradation depths in the DTG curve for hemicellulose, cellulose and lignin.

Table 3. Kinetic parameters determined using the Kissinger equation.

Component	Without Catalyst		With Catalyst	
	E (kJ/mol)	A (min^{-1})	E (kJ/mol)	A (min^{-1})
Hemicellulose	108.082	1.9×10^8	66.512	5.835×10^6
Cellulose	116.396	2.42×10^9	74.826	2.852×10^7
Lignin	182.908	2.98×10^{11}	133.024	1.460×10^9

Kinetic parameters from thermogravimetric data of the pyrolysis of peanut shells in the presence of a termite hill catalyst were also measured by applying the Kissinger method. The Kissinger plot drawn between $\ln B/T^2_m$ and $1000/T_m$ K^{-1} is depicted in Figure 6b, and E and A factor values are tabulated in Table 3. When activation energy values calculated from non-catalyzed and catalyzed reactions were compared, a clear difference was observed, which reflected the effectiveness of the catalyst and proved that a termite hill has a good catalytic ability to reduce the activation energy of the degradation reaction. The findings are in unison with earlier studies.

Xiang et al. [38] co-pyrolyzed lignocellulosic biomass with polyethylene over Co/ZSM-5. The authors reported an improvement in the reaction rate and a reduction in the activation energy value with the incorporation of Co/ZSM-5. Loy et al. [39] examined the catalyzed and non-catalyzed reactions of rice husk. They applied different models to determine the kinetic parameters. By applying the Kissinger model, the authors found that the activation energy in the presence of a catalyst was 146.35 kJ·mol^{-1}, while in the absence of a catalyst, it was 152.3 kJ·mol^{-1}. It was concluded that using rice hull ash as a catalyst reduced the activation energy during the pyrolysis reaction of lignocellulosic biomass.

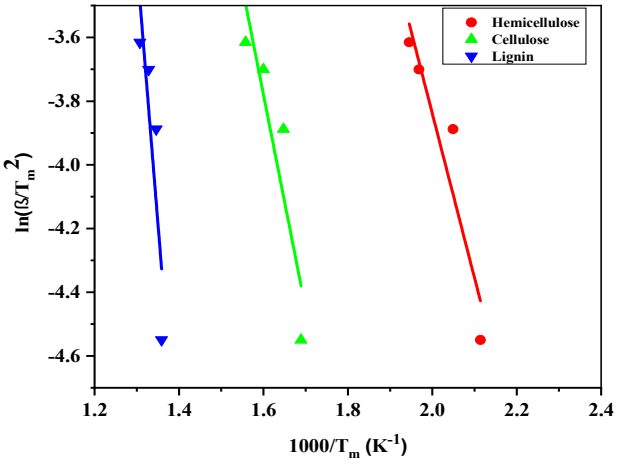

(**a**)

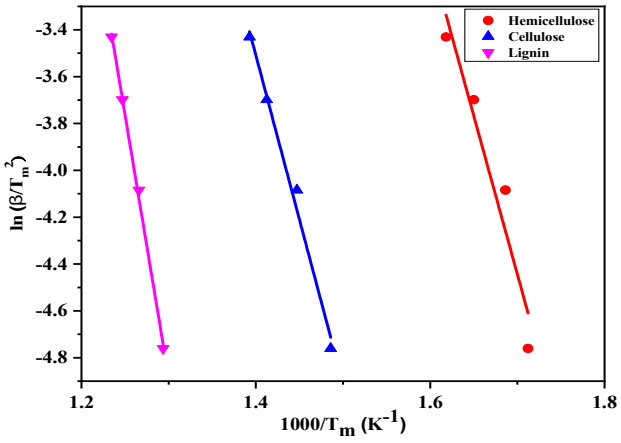

(**b**)

Figure 6. Kissinger plots obtained from pyrolysis of peanut shells (**a**) without a catalyst and (**b**) with a catalyst.

4. Conclusions

The results of our experiments reveal the pyrolytic conversion of waste peanut shells to useful products using a termite hill as the catalyst. A Pyrex vessel was used for sample insertion in an indigenously manufactured salt bath for pyrolytic degradation of catalyzed and non-catalyzed samples in an inert atmosphere in the temperature range of 310–380 °C. To study the nature of the oil obtained, GC-MS analysis was carried out. The oil obtained from the non-catalyzed reaction was found to comprise 2-methoxy-phenol, 2-furanmethanol, 2-methoxy-4-phenol, furfural, 2-methoxy-4-vinylphenol,4-ethyl-2-methoxy-phenol and lactose, while in the catalyzed reaction, 1-(4-hydroxy-3-methoxyphenyl)-propanone, tetrahydro[2,2′]bifuranyl-5-one, 1,2-benzenediol, cyclopropyl carbinol and 1-(4-hydroxy-3-methoxyphenyl)-ethanone were found in abundance.

To determine the kinetic parameters of the pyrolysis reaction of peanut shells in the presence/absence of a termite hill, thermogravimetry was performed in a N_2 environment at heating rates of 3, 12, 20 and 30 °C/min in the temperature range of 30 to 800 °C. The Kissinger method was applied to the TG data to calculate kinetic parameters. E and A values for the non-catalyzed reaction were calculated as 108.082, 116.396 and 182.908 kJ/mol and 1.9×10^8, 2.42×10^9 and 2.98×10^{11} min^{-1}, whereas for the catalyzed reaction, E and A values were calculated as 66.512, 74.826 and 133.024 kJ/mol, and 5.83×10^6, 2.859×10^7

and 1.46×10^9 min^{-1}, for hemicellulose, cellulose and lignin degradation, respectively. These differences in E and A values reflect the good catalytic properties of termite hills.

Author Contributions: J.N.: conceptualization, funding acquisition, resources, project administration. A.A.: investigation, methodology, writing—original draft. G.A. and N.U.R.: writing, results, analysis. A.S.: visualization, writing—review and editing. I.S.: funding acquisition, writing—review and editing. All authors have read and agreed to the published version of the manuscript.

Funding: Iltaf Shah graciously acknowledges the generous support of UAE University (SDG-Grant-2022). Jan Nisar acknowledges the support of the Higher Education Commission of Pakistan through grant No. 20–1491.

Conflicts of Interest: The authors have no conflict of interest.

References

1. Demirbas, A. Recent advances in biomass conversion technologies. *Energy Edu. Sci. Technol.* **2000**, *6*, 19–40.
2. Alhumade, H.; da Silva, J.C.G.; Ahmad, M.S.; Çakman, G.; Yıldız, A.; Ceylan, S.; Elkamel, A. Investigation of pyrolysis kinetics and thermal behavior of Invasive Reed Canary (Phalaris arundinacea) for bioenergy potential. *J. Anal. Appl. Pyrolysis* **2019**, *140*, 385–392. [CrossRef]
3. Gupta, S.; Gupta, G.K.; Mondal, M.K. Slow pyrolysis of chemically treated walnut shell for valuable products: Effect of process parameters and in-depth product analysis. *Energy* **2019**, *181*, 665–676. [CrossRef]
4. Farhad, S.; Saffar-Avval, M.; Younessi-Sinaki, M. Efficient design of feedwater heaters network in steam power plants using pinch technology and exergy analysis. *Int. J. Energy Res.* **2008**, *32*, 1–11. [CrossRef]
5. Danje, S. *Fast Pyrolysis of Corn Residues for Energy Production*; Stellenbosch University: Stellenbosch, South Africa, 2011.
6. Anspaugh, L.R.; Catlin, R.J.; Goldman, M. The global impact of the Chernobyl reactor accident. *Science* **1988**, *242*, 1513–1519. [CrossRef]
7. Zinkle, S.J.; Was, G. Materials challenges in nuclear energy. *Acta Mater.* **2013**, *61*, 735–758. [CrossRef]
8. Rathore, N.S.; Panwar, N. *Renewable Energy Sources for Sustainable Development*; New India Publishing: Delhi, India, 2007.
9. Lusas, E. Food uses of peanut protein. *J. Am. Oil Chem. Soc.* **1979**, *56*, 425–430. [CrossRef]
10. Torres-García, E.; Ramírez-Verduzco, L.; Aburto, J. Pyrolytic degradation of peanut shell: Activation energy dependence on the conversion. *Waste Manag.* **2020**, *106*, 203–212. [CrossRef]
11. Zhang, C.; Zhang, R.; Li, X.; Li, Y.; Shi, W.; Ren, X.; Xu, X. Bench-scale fluidized-bed fast pyrolysis of peanut shell for bio-oil production. *Environ. Prog. Sustain. Energy* **2011**, *30*, 11–18. [CrossRef]
12. Messina, L.G.; Bonelli, P.R.; Cukierman, A.L. Effect of acid pretreatment and process temperature on characteristics and yields of pyrolysis products of peanut shells. *Renew. Energy* **2017**, *114*, 697–707. [CrossRef]
13. Mamaeva, A.; Tahmasebi, A.; Yu, J. The effects of mineral salt catalysts on selectivity of phenolic compounds in bio-oil during microwave pyrolysis of peanut shell. *Korean J. Chem. Eng.* **2017**, *34*, 672–680. [CrossRef]
14. Nisar, J.; Rahman, A.; Ali, G.; Shah, A.; Farooqi, Z.H.; Bhatti, I.A.; Iqbal, M.; Ur Rehman, N. Pyrolysis of Almond Shells Waste: Effect of Zinc Oxide on Kinetics and Product Distribution. *Biomass Convers. Biorefinery* **2020**, 1–13. [CrossRef]
15. Kissinger, H.E. Variation of peak temperature with heating rate in differential thermal analysis. *J. Res. Natl. Bur. Stand.* **1956**, *57*, 217–221. [CrossRef]
16. Millogo, Y.; Hajjaji, M.; Morel, J.C. Microstructure, physical and mechanical properties of clayey material from termite mound: A stabilized material for adobe building. *Appl. Clay Sci.* **2011**, *51*, 160–164. [CrossRef]
17. Ayanda, O.S.; Amodu, O.S.; Adubiaro, H.; Olutona, G.O.; Ebenezer, O.T.; Nelana, S.M.; Naidoo, E.B. Effectiveness of termite hill as an economic adsorbent for the adsorption of alizarin red dye. *J. Water Reuse Desalination* **2019**, *9*, 83–93. [CrossRef]
18. Mahamat, A.A.; Azeko, S.T. Mechanical and structural properties of termite soil as a partial replacement to cement for different applications. *Mater. Sci.* **2018**, *2*, 1. [CrossRef]
19. Yusuff, A.S.; Azeez, T.M.; Babatunde, E.O. Titania-termite hill composite as a heterogeneous catalyst: Preparation, characterization, and performance in transesterification of waste frying oil. *Int. J. Chem. React. Eng.* **2020**, *18*, 10–11. [CrossRef]
20. Yusuff, A.S. Photocatalytic degradation of cationic dye in aqueous solution by TiO_2 nanoparticle immobilized on termite hill soil. *React. Kinet. Mech. Catal.* **2020**, *131*, 979–995. [CrossRef]
21. Folorunso, D.; Aribo, S.; Olaniran, O. Performance Evaluation of Insulating Firebricks Produced from Hydrometallurgically Purified Termite Hill Clay Reinforced with Alumina. *Am. J. Eng. Res.* **2015**, *4*, 1–7.
22. Yusuff, A.S.; Bello, K.A.; Azeez, T.M. Photocatalytic degradation of an anionic dye in aqueous solution by visible light responsive zinc oxide-termite hill composite. Reaction Kinetics. *Mech. Catal.* **2020**, *131*, 537–554.
23. Zanardi, S.; Cruciani, G.; Alberti, A.; Galli, E. Dehydration and rehydration process in boggsite: An in situ X-ray single-crystal study. *Am. Mineral.* **2004**, *89*, 1033–1042. [CrossRef]
24. Dent, L.; Smith, J. Crystal structure of chabazite, a molecular sieve. *Nature* **1958**, *181*, 1794–1796. [CrossRef]
25. Burt, J.B.; Ross, N.L.; Angel, R.J.; Koch, M. Equations of state and structures of andalusite to 9.8 GPa and sillimanite to 8.5 GPa. *Am. Mineral.* **2006**, *91*, 319–326. [CrossRef]

26. Gao, M.Y.; Wang, F.; Gu, Z.G.; Zhang, D.X.; Zhang, L.; Zhang, J. Fullerene-like Polyoxotitanium cage with high solution stability. *J. Am. Chem. Soc.* **2016**, *138*, 2556–2559. [CrossRef]
27. Zachariasen, W. Skrifter utgitt av det Norske Videnskaps Akademi i Oslo 1: Matematisk Naturvidenskapelig Klasse. 1928.
28. Swamy, V.; Dubrovinsky, L.S.; Dubrovinskaia, N.A.; Langenhorst, F.; Simionovici, A.S.; Drakopoulos, M.; Dmitriev, V.; Weber, H.P. Size effects on the structure and phase transition behavior of baddeleyite TiO_2. *Solid State Commun.* **2005**, *134*, 541–546. [CrossRef]
29. Pecharromán, C.; Gonzalez-Carreno, T.; Iglesias, J.E. The infrared dielectric properties of maghemite, γ-Fe_2O_3, from reflectance measurement on pressed powders. *Phys. Chem. Miner.* **1995**, *22*, 21–29. [CrossRef]
30. Scherrer, P. *Bestimmung der Inneren Struktur und der Größe von Kolloidteilchen Mittels Röntgenstrahlen, Kolloidchemie Ein Lehrbuch*; Springer: Berlin/Heidelberg, Germany, 1912; pp. 387–409.
31. Millogo, Y.; Hajjaji, M.; Morel, J. Physical properties, microstructure and mineralogy of termite mound material considered as construction materials. *Appl. Clay Sci.* **2011**, *52*, 160–164. [CrossRef]
32. Mujinya, B.B.; Mees, F.; Erens, H.; Dumon, M.; Baert, G.; Boeckx, P.; Ngongo, M.; Van Ranst, E. Clay composition and properties in termite mounds of the Lubumbashi area, DR Congo. *Geoderma* **2013**, *192*, 304–315. [CrossRef]
33. Pütün, E.; Uzun, B.B.; Pütün, A.E. Production of bio-fuels from cottonseed cake by catalytic pyrolysis under steam atmosphere. *Biomass Bioenergy* **2006**, *30*, 592–598. [CrossRef]
34. Aho, A.; Kumar, N.; Eränen, K.; Salmi, T.; Hupa, M.; Murzin, D.Y. Catalytic pyrolysis of woody biomass in a fluidized bed reactor: Influence of the zeolite structure. *Fuel* **2008**, *87*, 2493–2501. [CrossRef]
35. Messina, L.G.; Bonelli, P.R.; Cukierman, A.L. In-situ catalytic pyrolysis of peanut shells using modified natural zeolite. *FuelProcessing Technol.* **2017**, *159*, 160–167.
36. Lopez-Velazquez, M.; Santes, V.; Balmaseda, J.; Torres-Garcia, E. Pyrolysis of orange waste: A thermo-kinetic study. *J. Anal. Appl. Pyrolysis* **2013**, *99*, 170–177. [CrossRef]
37. Yang, H.; Yan, R.; Chen, H.; Zheng, C.; Lee, D.H.; Liang, D.T. In-depth investigation of biomass pyrolysis based on three major components: Hemicellulose, cellulose and lignin. *Energy Fuels* **2006**, *20*, 388–393. [CrossRef]
38. Xiang, Z.; Liang, J.; Morgan, H.M., Jr.; Liu, Y.; Mao, H.; Bu, Q. Thermal behavior and kinetic study for co-pyrolysis of lignocellulosic biomass with polyethylene over Cobalt modified ZSM-5 catalyst by thermogravimetric analysis. *Bioresour. Technol.* **2018**, *247*, 804–811. [CrossRef]
39. Loy, A.C.M.; Gan, D.K.W.; Yusup, S.; Chin, B.L.F.; Lam, M.K.; Shahbaz, M.; Unrean, P.; Acda, M.N.; Rianawati, E. Thermogravimetric kinetic modelling of in-situ catalytic pyrolytic conversion of rice husk to bioenergy using rice hull ash catalyst. *Bioresour. Technol.* **2018**, *261*, 213–222. [CrossRef] [PubMed]